

SEISMIC PROTECTION OF ARTEFACTS WITH ADHESIVES AND BASE-ISOLATION

**Claire Dong¹, Giovanni De Francesco², Timothy Sullivan³,
Rajesh P. Dhakal⁴, Terri Elder⁵, Emily Fryer⁶ and
Neeha Velagapudi⁶**

(Submitted July 2022; Reviewed October 2022; Accepted January 2023)

ABSTRACT

Artefacts in museums, galleries, and private collections have great cultural value. In regions with high seismicity, earthquake shaking can pose significant risk of irreversible damage to such pieces. Various seismic protection methods have been proposed in the past for different types of artefacts. This study investigates one of the commonly used methods in New Zealand which consists in applying adhesives to anchor relatively small artefacts. Guidance is provided to determine the size and number of adhesives required for an artefact to survive design-level earthquake shaking. In addition, for large objects where adhesives alone are insufficient, a simple cost-effective base-isolation platform is proposed to reduce the seismic vulnerability of the artefacts. This platform is designed such that it can be assembled and positioned by museum conservators or private collectors. The adhesive material properties are determined through direct tension and shear experimental tests. The friction properties of the base-isolated substrate are determined through unidirectional quasi-static and cyclic load tests. Performance of the proposed methodology is gauged by subjecting the artefacts to shake table testing using a recorded earthquake motion. Results suggest that the recommended seismic protection solution performs as expected.

<https://doi.org/10.5459/bnzsee.1613>

INTRODUCTION

Seismic events pose threats to artefacts in museums and art galleries, and this has been verified in recent large earthquake events around the world. For example, the 1997-1998 Umbria-Marche earthquakes damaged 3150 movable artefacts, the 2009 L'Aquila earthquakes, the 2010-2011 Canterbury earthquakes, and many others have all caused uncountable losses to cultural heritage [1]. Recently, progress has been made in developing low damage seismic design solutions for buildings [2,3], but even for a building with high seismic resilience, there is still a chance of damage to contents. The contents displayed in museums and art galleries are considered as acceleration-sensitive non-structural components, whose current design practice needs improvement [4]. Various protection methods have been proposed for artefacts: the silicon dampers between cabinet stored cultural relics [5], waxes for small to medium sized fragile objects [6], and base isolation devices such as frictional and elastomeric isolators for large statues [7-10]. Most of the proposed seismic protection methods are prescribed for certain types of artefacts and there are constraints to when they may be applied. For example, waxes are not sufficient to anchor large statues, an elastomeric bearing device will not be activated with light-weighted objects, and isolation devices in general require a decent amount of clearance to prevent the impact with the surroundings.

In New Zealand, museums, galleries, and private collectors, custom mounts, bent wires, walker pins, weights, and various types of adhesives are typical restraint solutions. However, a lack of adequate documentation regarding the performance of adhesive methods has raised concerns [11]. The Canterbury Museum initiated a series of studies to investigate various restraint methods including adhesives and examined two

aspects of their performance. The first aspect is related to conservation and display standards. A good restraint method should minimise the damage to artefacts, should be easy to apply and remove, and not affect the aesthetic of displayed objects. A qualitative assessment was carried out to test the removability and residual of various adhesives by the Canterbury Museum [11], the results showed that Lascaux 303HV, Rhoplex N-580, and Lascaux 303HV mixtures had the good removability with minimal residues. The second aspect is the effectiveness of protecting artefacts during an earthquake. Preliminary tests were performed by the Canterbury Museum using shake table and tilt table [11]. However, these tests were not able to quantify the strength of adhesives.

This research has been developed in collaboration with the Canterbury Museum to further investigate and quantify the characteristics of two adhesives (Lascaux 303HV and Rhoplex N-580) that were recommended by the Canterbury Museum and provide guidance on installation procedures. Worth noting that Rhoplex N-580 has been a commonly used adhesive in museums and galleries, but its manufacture was discontinued in 2018. Tension and shear tests are used to determine the strength and stiffness of the adhesives, which influences the capacity to resist earthquake shaking. Seismic demand is estimated based on elastic floor response spectra. Comparing the capacity and demand, the number and size of adhesives required to anchor an object, can be estimated. Furthermore, it is expected that adhesives would only work for small objects (e.g. objects that are less than 4 to 5 kgs). For medium to large objects where adhesives alone are not sufficient to withstand an earthquake, an affordable frictional base-isolated substrate is proposed. Unidirectional and cyclic load tests are carried out to determine the friction coefficient of the base-isolator.

¹ Corresponding Author, PhD candidate, University of Canterbury, Christchurch, claire.dong@pg.canterbury.ac.nz (Member)

² Postdoctoral Fellow, University of Canterbury, Christchurch, giovanni.defrancesco@canterbury.ac.nz

³ Professor, University of Canterbury, Christchurch, timothy.sullivan@canterbury.ac.nz (Member)

⁴ Professor, University of Canterbury, Christchurch, rajesh.dhakal@canterbury.ac.nz (Fellow)

⁵ Researcher, University of Canterbury Teece Museum and James Logie Memorial Collection, Christchurch

⁶ Researcher, Canterbury Museum, Rolleston Avenue, Christchurch

ADHESIVE TEST PROCEDURE AND SETUP

Test Specimens

Experimental tests were conducted to determine the adhesive tensile strength, tensile stiffness, shear strength, and shear stiffness. Four adhesives were prepared by the Canterbury Museum laboratory: Rhoplex N-580, Lascaux 303HV, and two mixtures. These two mixtures contain Lascaux 303HV, Lascaux 498HV, and H₂O with ratios of 2:0:1 and 9:1:5, respectively. The adhesive dots were prepared following the instructions given by the Canterbury Museum. Figure 1 presents the steps to make adhesive dots. Figure 1a shows a template that contains circles with diameters of 10 mm, 6 mm, 3 mm, and 1 mm (in this study referred to as D10, D6, D3, and D1, respectively). Figure 1b shows the adhesives just after pipetting onto a non-stick paper (e.g. baking paper) using a syringe. The dots are then carefully covered with another sheet of baking paper and left to dry (Figure 1c). The final product is shown in Figure 1d. The dot thickness is not specifically controlled, but the thickness of the samples formed via this process was fairly constant at around 0.5-2.0 mm depending on the diameter. The drying duration depends on the water content and varies between adhesives. Lascaux 303HV and its mixtures may take one to two days to dry, whereas Rhoplex N-580 can take up to five days. The prepared adhesive dots are then applied to the base of an object and placed on top of a substrate. Ceramics and glass are common materials among artefact collections. Glass, acrylic, and painted medium density fibreboard (MDF) are commonly used as substrates. Objects made from these materials were tested to replicate typical objective-adhesive-substrate conditions in museums. Examples of tested specimens are shown in Figure 2.

Tension and Shear Test Setups

Direct tension and shear tests have been conducted at the University of Canterbury using a universal testing machine, as illustrated in Figure 3. A string was hung from the load cell and tied to the object. The string was made of ultra-high-molecular-weight polyethylene (UHMWP) fibres and had an extremely high stiffness; therefore, its elastic deformation was considered negligible under a small load test [12]. The vase is anchored onto the substrate using adhesive dots. The test was displacement controlled, with a loading rate of 20 mm/min. A transducer was attached to the testing frame to measure the vertical displacement. The direct shear test is described in

Figure 4. The test object was subjected to a horizontal force from the pulley on one side and attached to the transducer on the other side. The force was applied as close to the base as possible to minimise the overturning moment.

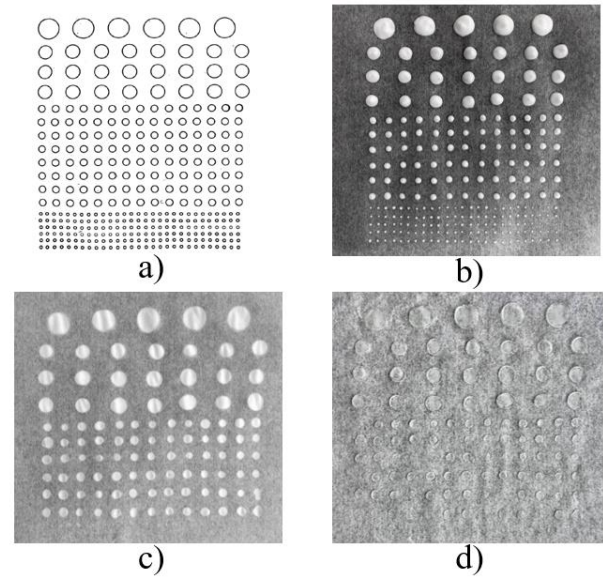


Figure 1: Adhesive dots preparation procedures: a) a template of the sizes, b) pipet adhesive with a syringe, c) cover with baking paper, and d) final product.



Figure 2: Specimens and substrates used to test the adhesives: a) ceramic vase, terracotta pot, wine glass, flat glass, b) acrylic substrate, and c) painted MDF substrate.

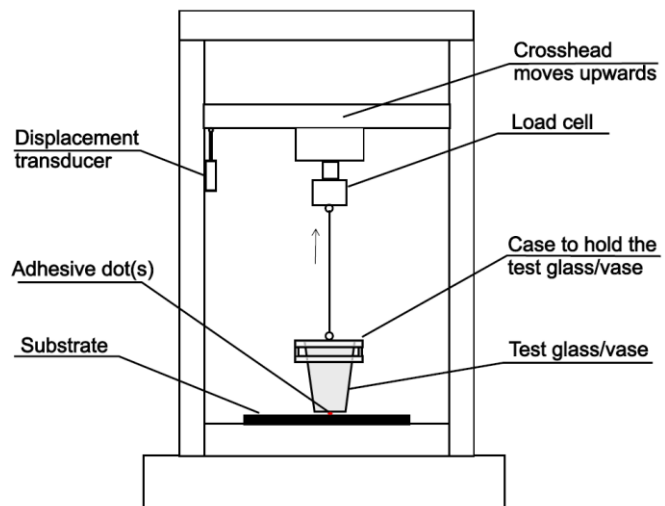


Figure 3: Direct tension test to determine adhesives' tensile properties.

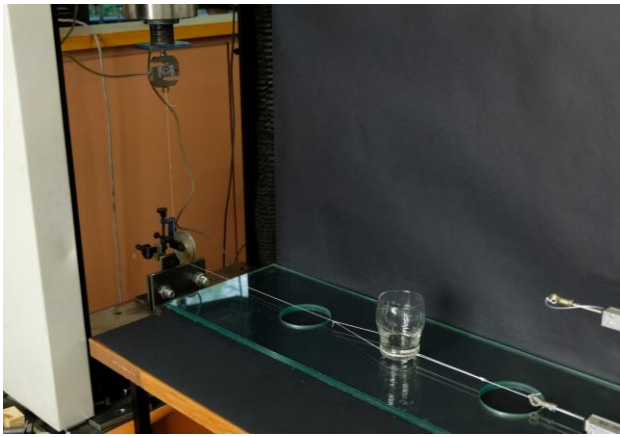


Figure 4: Direct shear test to determine adhesives' shear properties.

Adhesive Test Groups

For each test setup, three test groups were scheduled to investigate different characteristics of adhesives. Consider the variation in the adhesive properties, each individual test is repeated five times. Test group A determined the characteristic strength and stiffness of adhesives dots. To eliminate possible impacts from applying multiple dots and different contact surfaces, a single dot between the glass object and glass substrate was used for all tests in group A. The independent variable in group A was the type of adhesive dot (four types of adhesives with four diameters), summarised in Table 1. Due to the time constraints, only D6 was tested for Lascaux 303HV mixtures, which was sufficient to determine the effectiveness of adding Lascaux 498HV and water.

Table 1: Test group A – investigate the strength and stiffness of adhesive dots.

Adhesives	Tension test	Shear test
Lascaux 303HV	D1, D3, D6, D10	D1, D3, D6, D10
Rhoplex N-580	D1, D3, D6, D10	D1, D3, D6, D10
Mixture 1* (2:0:1)	D6	D6
Mixture 2* (9:1:5)	D6	D6

* Mixtures of Lascaux 303HV, Lascaux 498HV, and H₂O, respectively, with specified mixing ratios.

Test group B investigated the effects of adhesives on various contact surfaces. Thus, the independent variable was the object and substrate materials, while the type of adhesive, dot size, and the number of dots remained the same. One Lascaux 303HV D6 dot was applied to a few combinations; glass-glass (glass object on glass substrate), glass-acrylic, glass-MDF, terracotta-glass, and ceramic-MDF.

Test group C was developed to investigate the effect of applying multiple dots under tension and shear. It was necessary to determine whether the strength is proportional to the number of applied dots. The independent variable was the number of applied dots. One, two, and four Lascaux 303HV D6 dots were applied between the glass object and the glass substrate with the configurations shown in Figure 5.

TEST PROCEDURE OF BASE-ISOLATED SUBSTRATE

Proposed Low-Cost Base-Isolation System

Adhesives are a practical solution for smaller artefacts that are commonly subjected to low seismic demand. However, for relatively larger objects, such as the ceramic vase shown in

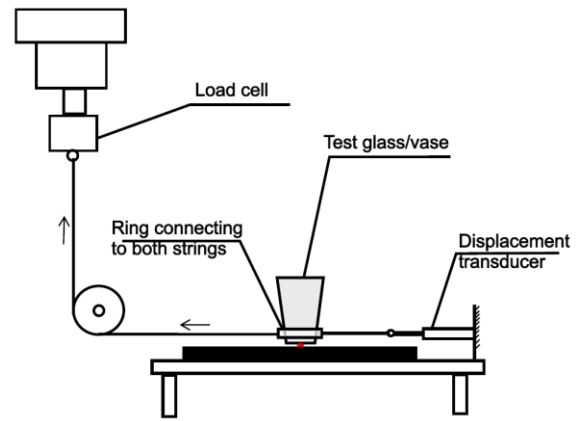


Figure 2, using adhesives alone is not sufficient. In this study, for the cases where adhesives-only are not a suitable solution, a base-isolated substrate is proposed (see Figure 6). This device comprises a rigid board that acts as the substrate for artefacts, with four small pieces of flat Polytetrafluoroethylene (PTFE) glued at each corner. PTFE is a low-friction material also used for friction devices of base-isolated buildings. Similar to a seismic isolator used in the building design, the base-isolated substrate limits the seismic force transferred into the artefact above. It is free to slide on the bearing during a seismic event, therefore, adequate clearance should be provided based on the displacement demand (calculated in later sections) to avoid impact with the surroundings. Self-centring could be considered, but it is not essential as the substrate can be centred manually after an earthquake.

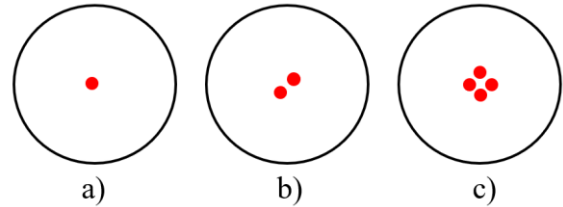


Figure 5: Test group C – configurations of multiple dots applied at the base of the glass.

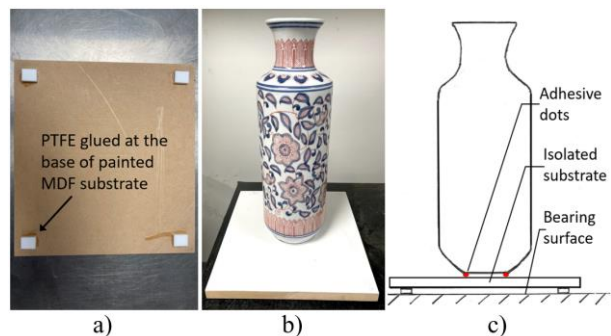


Figure 6: Proposed design of the affordable base-isolated substrate: a) view from the bottom, b) and c) are front views with a vase on top.

Tests were carried out to determine its static friction (μ_{static}) and dynamic ($\mu_{dynamic}$) friction coefficients, which are then used to compute the seismic force and displacement demands. The coefficient of friction can be dependent on the roughness of the bearing surface, sliding speed, normal stress, temperature, and other parameters [13].

Determine the Coefficient of Friction via Unidirectional Loading Tests

To provide insight into the coefficient of friction, similar to a conventional friction test, a pulley was first added to the universal testing machine to enable a quasi-static friction test, as illustrated in Figure 7. As the load cell moved up, a horizontal force was applied to the device through the string with unidirectional loading. The displacement was recorded by a horizontal transducer. The friction coefficient between PTFE and three bearing surfaces; glass, acrylic, and stainless steel, were investigated. Painted MDF was not tested because the paint was easily worn out from repeated friction sliding. All surfaces were dried and cleaned without any lubricant. The tests were displacement controlled at speeds of 5 and 100 mm/min to investigate the effects of speed, even though the test speed was still relatively low. The effects of weight were tested by adjusting the overall mass from 2 to 6 kg (corresponding to normal stress of 10.9 to 32.7 MPa) with an increment of 1 kg.

This range of mass is roughly what is expected in small a museum display. In all the cases examined the normal stress acting on the PTFE was less than 0.03 MPa.

Determine the Coefficient of Friction via Cyclic Loading Tests

The unidirectional test described above provided an indication of the friction coefficient at low sliding speeds. However, considering that the base-isolated substrate was intended to slide under seismic excitation, it was also deemed necessary to investigate the sensitivity of the friction coefficient to dynamic response. Figure 8 illustrates a friction test setup on the shake table where PTFE was subjected to cyclic loading. The same base-isolated substrate was tested with a total weight of 4 kg. The shake table was displacement controlled by imposing sinusoidal waves with frequencies of 0.01, 0.1, 0.3, 1, and 2 Hz, corresponding to maximum sliding speeds of 4, 35, 93, 280, and 415 mm/s, respectively.

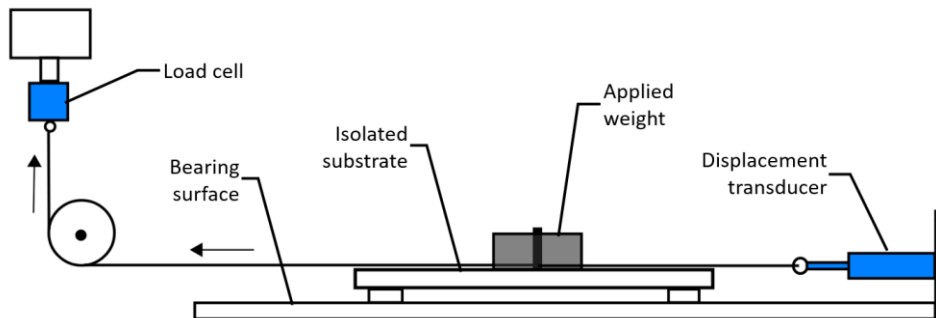
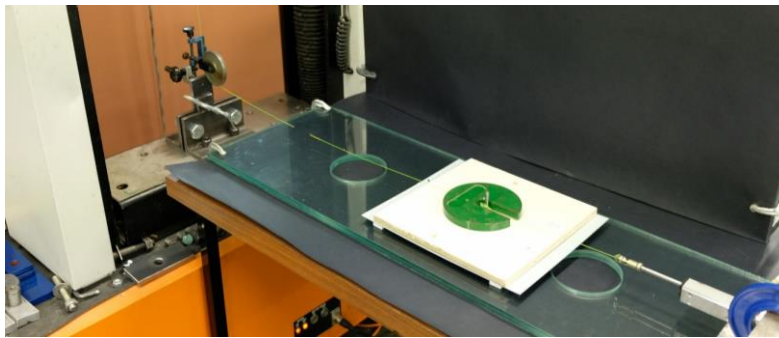


Figure 7: Unidirectional friction test setup to determine static and dynamic friction of coefficients.

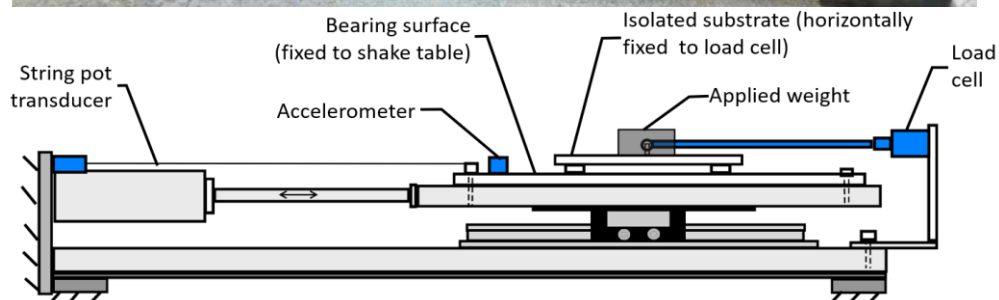


Figure 8: Dynamic friction test set-up for an artefact isolation system via use of a shake table.

MECHANICAL PROPERTIES OF ADHESIVES

Characteristic Strength and Stiffness of Adhesives

The characteristic strength and stiffness of each type of adhesive were determined by Test group A. Recall that Test group A had a single dot between a glass object and glass substrate. Figure 9 plots the force-displacement curves for four sizes of Lascaux 303HV dots (other adhesives share similar behaviour and so are not presented here). Detailed experimental results are documented separately [14]. Initially, elastic behaviour was observed under both tension and shear. Once the peak strength was reached, the tensile strength rapidly reduced to zero, and debonding occurred between the adhesive and the contact surface. This means that the tensile strength is sensitive to displacement, with just a small increase in post-peak displacement potentially leading to complete loss of strength. Shear strength degradation also occurred; a residual strength was observed because the adhesive ended up rolling between two surfaces. In Figure 9a, all adhesives reached their peak resistance at around 1 mm of displacement, suggesting the stiffness and strength are dependent on the size of the dot.

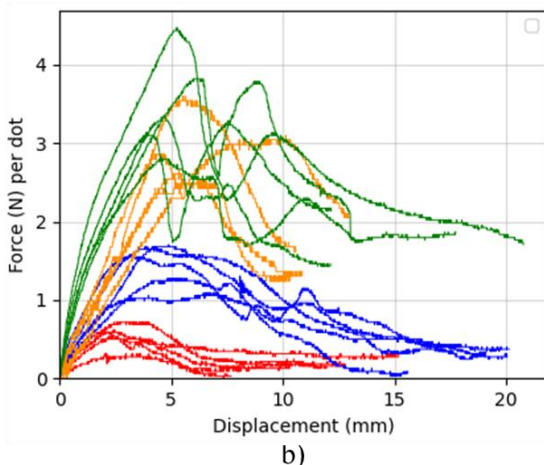
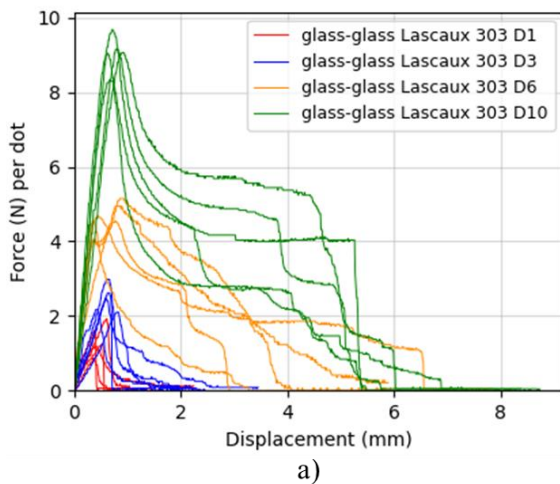


Figure 9: Force-displacement curves for glass objects on glass substrates for a single Lascaux 303HV dot: a) tension test results, b) shear test results.

The distributions of adhesive strength and stiffness are developed using the mathematical procedure (Method A) provided by Porter et al. [15]. This method creates a fragility function for a certain damage state, given that all tested specimens have reached that damage state and the Engineering Demand Parameters (EDPs) are known. In this study, the damage state is defined as the rapid strength degradation once the peak strength is reached, and the EDP is the peak tensile or

shear strength. The five data points from each test set are used to fit the fragility function. In addition, Porter et al. [15] suggests that the fragility function should be tested using a goodness-of-fit test and is accepted if it passes at the 5% significance level. Lilliefors test [16] is a goodness-of-fit test developed based on the Kolmogorov-Smirnov test. It is more suitable than the K-S test when the population's parameters are unknown. All fitted fragility functions have passed the Lilliefors test with a 95% confidence interval, an example is shown in Figure 10.

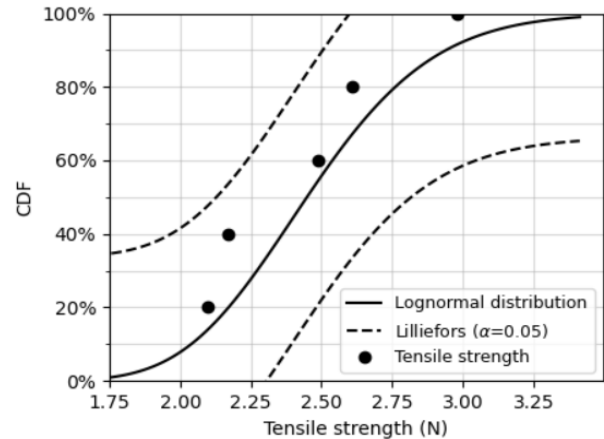


Figure 10: Fitted fragility function and five test results from glass-glass Lascaux 303 D3.

The characteristic tensile and shear strength are defined by the 5th percentile values, whereas the characteristic tensile and shear stiffness are defined by the median values. All test results are reported in Table 2. The strength of each adhesive dot varies because of imperfections that arise during dot preparation (e.g., not perfectly circular or slightly different sizes). This variability appears unavoidable and should be tolerated by adopting a conservative number of dots. Future research should investigate a more rigorous and uniform way of preparing adhesive dots to reduce variability. Comparing the strength values across different diameters, they are not proportional to the area of the dot, but more correlated to the diameter (or perimeter). The initial stiffness is obtained by computing the gradient of the force-displacement curve within the elastic region and then taking the mean value of five tests as the initial stiffness.

Variability of Adhesive Strength on Different Surfaces

The variability of adhesive strength on different contact surfaces is studied by test group B which had a single Lascaux 303HV D6 dot applied between various objects and substrates. A comparison of the 5th percentile strength is shown in Table 3. The results obtained suggest that coarse surfaces like terracotta and painted MDF tend to have a slightly lower tensile strength, but this difference is less significant compared to the strength variation. The shear strength does not show a trend between coarse and smooth surfaces. Both tensile and shear stiffness vary significantly.

Effects of Applying a Group of Adhesive Dots

The effects of applying multiple adhesive dots are investigated in test group C, which had the same adhesives and specimens but with one, two, and four dots. Average strength and stiffness per dot are compared in Table 4. The tensile strength is seen to decrease as the number of dots increases. This behaviour was further investigated by applying the same number of dots but spaced out. For example, Figure 11 shows an extreme case where two dots were applied as far apart as possible. Instead of engaging simultaneously, one reached its peak and lost strength first, the second dot then engaged. A reasonable explanation

Table 2: Strength at the 5th percentile and mean stiffness for various adhesives between glass objects and glass substrates.

Adhesives	Dot Size	Tensile strength [N]	Shear strength [N]	Tensile stiffness [N/mm]	Shear stiffness [N/mm]
Lascaux 303HV	D1	0.80	0.32	3.41	0.31
	D3	1.94	1.05	3.97	0.58
	D6	4.36	2.34	12.96	0.60
	D10	8.29	2.63	14.13	1.27
Rhoplex N-580	D1	0.99	0.28	3.28	0.19
	D3	1.14	0.63	5.62	0.46
	D6	3.38	1.25	6.57	0.91
	D10	6.74	2.24	14.72	1.17
Mixture 1* (2:0:1)	D6	2.59	1.68	3.27	1.15
Mixture 2* (9:1:5)	D6	1.87	2.51	3.62	1.32

* Mixtures of Lascaux 303HV, Lascaux 498HV, and H₂O, respectively, with specified maxing ratios.

Table 3: Strength at the 5th percentile and mean stiffness for different surfaces.

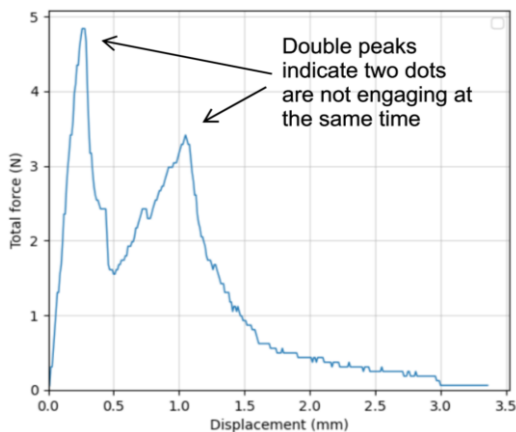
	Tensile strength [N]	Shear strength [N/mm]	Tensile stiffness [N]	Shear stiffness [N/mm]
Glass-glass	4.36	2.34	12.96	0.60
Glass-acrylic	5.32	2.17	9.72	1.03
Glass-MDF	3.88	2.03	13.14	0.86
Terracotta-glass	4.11	2.03	4.78	0.71
Ceramic-MDF	4.08	2.51	16.64	1.03

Table 4: Multiple-dot test using Lascaux 303HV D6 between glass objects and glass substrates.

	Tensile strength [N]	Shear strength [N]	Tensile stiffness [N/mm]	Shear stiffness [N/mm]
1 dot	4.36 (4.36)	2.34 (2.34)	12.96 (12.96)	0.60 (0.60)
2 dots	7.86 (3.93)	4.28 (2.14)	7.14 (3.57)	2.00 (1.00)
4 dots	14.60 (3.65)	9.44 (2.36)	9.38 (2.34)	3.82 (0.95)

Note: the values in brackets are normalised for per dot

would be that adhesive dots are sensitive to displacement imposed after peak strength and when spaced out, they are more likely to be subjected to different vertical displacements (owing to the eccentric loading) and reach their peak strength one after the other. In this case, the total tensile strength is not proportional to the number of dots.

**Figure 11: Tensile force-displacement curve where two adhesive dots are applied as far as possible.**

FRICITION TEST RESULTS AND DISCUSSION

Test Results from Unidirectional Loading Tests

For the friction-sliding base-isolation system, the static and dynamic coefficients of friction (μ_{static} and μ_{dynamic}) determined using the unidirectional tests described in previous section are summarised in Figure 12, where each point represents the average value of two repeated tests. The detailed experimental results are documented separately [17]. The test results show that PTFE-acrylic has a coefficient of friction, μ , between 0.09 – 0.2. PTFE-glass and PTFE-stainless steel have similar μ , around 0.06 – 0.12. The comparison between μ_{static} and μ_{dynamic} shows that the value of μ_{static} is always higher and has a relatively large variability. There is no clear evidence that μ varies with different weights in the unidirectional tests. One possible reason could be that the applied normal stress is too small (all less than 0.03 MPa). The experimental test results in the literature have shown that μ decreases with an increase in normal stress [13,18], and this change is observed over a range of normal stress from 5 to 45 MPa. Therefore, considering that the museum artefacts included in this study are unlikely to impose high normal stress variation, it is acceptable to conclude that the variation in weight does not have a significant effect on the coefficient of friction. With an increase in sliding speed, a

higher μ should be expected [12,19]. This phenomenon is captured by the unidirectional test in Figure 12, where dotted lines represent a sliding speed of 5 mm/min (0.08 mm/s) and solid lines represent 100 mm/min (1.67 mm/s).

Test Results from Cyclic Load Tests

Shake table friction tests have been conducted to determine the frictional behaviour under cyclic loads. Three materials were tested under five sinusoidal waves with frequencies of 0.01, 0.1, 0.3, 1, and 2 Hz, corresponding to maximum sliding speeds of 4, 35, 93, 280, and 415 mm/s, respectively. A typical force-displacement (expressed in terms of a friction coefficient vs displacement) curve, for PTFE sliding on stainless steel is plotted in Figure 13. The rest of the experimental results are documented separately [20]. In Figure 13a, the frequency of a complete cycle is 0.01Hz, and μ_{max} occurs at the maximum displacement. In Figure 13b, the frequency is 0.3 Hz, and μ_{max} occurs at the maximum and zero displacements. At the maximum displacement, the shake table changes its direction of movement, and the isolator is stationary for an instant and must overcome the static friction again. At zero displacement, the

shake table is moving at its maximum speed which corresponds to the highest $\mu_{dynamic}$.

A similar trend is observed in other results which are summarised in Figure 14, where μ_{static} and $\mu_{dynamic}$ are plotted against frequency and maximum sliding speed. Increasing the frequency and hence sliding speed, results in an increase in both μ_{static} and $\mu_{dynamic}$. The increasing rate of $\mu_{dynamic}$ is larger at low speeds and gradually flattens as speed gets higher. In practice, the relationship between $\mu_{dynamic}$ and speed is often modelled with an exponential component, which suggests that at very high speeds it will reach a steady $\mu_{dynamic}$ value [19], in this case 0.25 for PTFE-glass, PTFE-stainless steel, and 0.35 for PTFE-acrylic. μ_{static} exhibits similar behaviour. Compared to the values obtained from the unidirectional friction test, the friction coefficients obtained from dynamic tests are all higher. The friction coefficients between PTFE-glass and PTFE-stainless steel are very similar which makes glass a more suitable bearing surface than stainless steel because it is aesthetic and cost-efficient. Acrylic is not recommended as a base-isolation bearing surface because of its high friction coefficient.

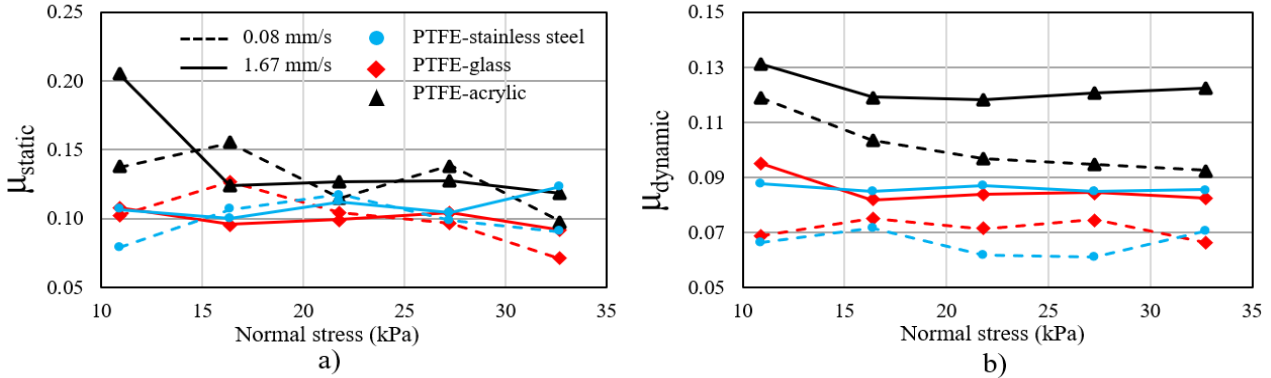


Figure 12: Unidirectional load friction test results: a) static coefficient of friction, and b) dynamic coefficient of friction.

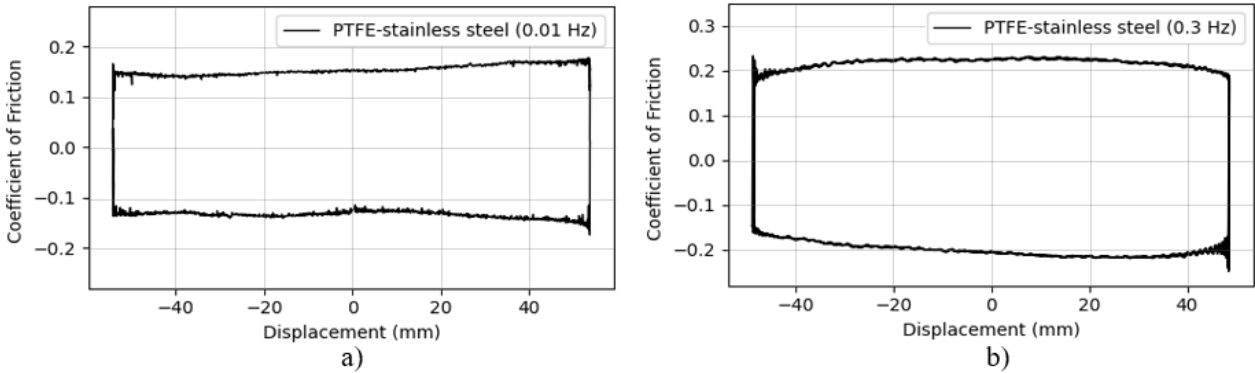


Figure 13: Cyclic load friction test results for PTFE sliding on stainless steel: a) hysteresis loop with a frequency of 0.01 Hz and b) frequency of 0.3 Hz.

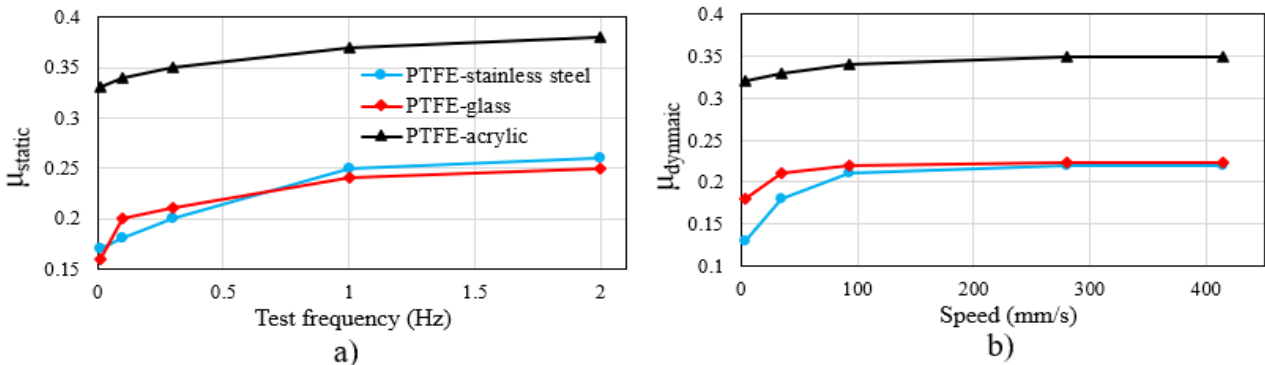


Figure 14: Cyclic load friction test results: a) static friction coefficient, and b) dynamic friction coefficient.

RECOMMENDATIONS ON INSTALLING ADHESIVE DOTS

The adhesive capacity of the dots can be calculated using the characteristic strength obtained from experimental testing. It is recommended to use the values reported in Table 2 (the 5th percentile strength between glass and glass surfaces) because they have been verified through testing and are thought to be representative of other tested surfaces. To compute the seismic demand, overturning and shear failure modes are considered in this section. The demand depends on a few parameters such as the weight of the artefacts and the local seismicity. A heavier object experiences a larger inertia force as a reaction to the acceleration produced by an earthquake. Another important parameter is the aspect ratio (ratio between height and width) of the object. For example, two objects with the same weight but different heights will be subjected to different overturning moment demands, as a result of differences in the height to the centre of mass (COM). Considering that objects can have different shapes and therefore to avoid the calculation of the COM, a simplification is made by defining two shape categories, see Figure 15, where B is the base width, L is the height to the COM, and H is the total height. If the shape of an object is similar to Figure 15a, then its COM is assumed to be at mid-height. If an object is shaped similarly to Figure 15b, then its COM is assumed to be at 2/3 of the height. Note that for simplicity it is also assumed that the artefacts are symmetrical around the base. The last important parameter required to calculate the seismic demand is the component spectral acceleration, which represents the maximum acceleration demand expected on a component during an earthquake. More details on this are discussed later.

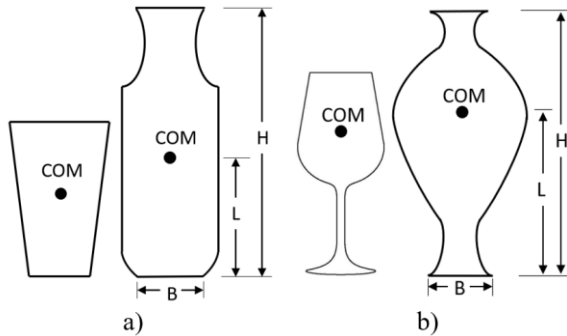


Figure 14: Different shapes of artefacts: a) centre of mass is assumed at half height; and b) centre of mass is assumed at 2/3 of the total height.

The forces experienced by the artefact during an earthquake are illustrated in Figure 16. Both the overturning and shear mechanisms need to be checked. For an object to begin overturning, its destabilising moment demand (M_D) has to exceed its stabilising moment capacity (M_C). The stabilising moment is provided by the artefact self-weight and the tensile resistance of the adhesive dots:

$$M_C = W \cdot \frac{B}{2} + N_{OT} \cdot T_i \cdot B \quad (1)$$

where W is the artefact weight, T_i is the characteristic tensile strength of the chosen adhesive dot, and N_{OT} is the number of dots on each side. Because earthquakes can strike from any direction, it is necessary to apply adhesives in four quadrants, and the total number of dots is $4N_{OT}$. Since the tensile strength of adhesive dots is sensitive to the displacement, the dots in each quadrant should be applied closely together and as far from the centre as possible to maximise the lever arm. The destabilising moment (M_D) due to earthquake shaking is:

$$M_D = F \cdot L = W \cdot SA_{NS} \cdot L \quad (2)$$

where F is the inertia force generated from ground shaking, SA_{NS} is the design seismic coefficient (spectral acceleration) demand for the non-structural component and L is the height to the COM (see Figure 15). The object is stable if the capacity, M_C is greater than the demand, M_D . Rearranging Equations 1 and 2 to obtain the following expression, which is used to determine the number of adhesive dots required in each quadrant to prevent overturning.

$$N_{OT} \geq \frac{W}{T_i} \left(\frac{L \cdot SA_{NS}}{B} - \frac{1}{2} \right) \quad (3)$$

Shear failure can occur when the object's COM is low (i.e. short and squat). The friction between the object and substrate is neglected as the surfaces are not likely in contact due to the thickness of the adhesive dots. The shear resistance capacity (V_C) is then:

$$V_C = 4N_s \cdot V_i \quad (4)$$

where V_i is the characteristic shear strength of the chosen adhesive dot and N_s is the number of dots in each quadrant, to be consistent with the overturning requirements. The shear demand (V_D) is:

$$V_D = F = W \cdot SA_{NS} \quad (5)$$

Again, the object is deemed stable when the shear resistance is greater than the demand. The following equation is derived from Equations 4 and 5, which gives the number of adhesive dots required in each quadrant to prevent shear failure.

$$N_s \geq \frac{SA_{NS} \cdot W}{4V_i} \quad (6)$$

Now, to ensure the adhesives provide sufficient overturning and shear capacities, the required number and size of the adhesives should be chosen conservatively (i.e. larger of N_{OT} or N_s), as suggested by Equation 7.

$$N = \max \left\{ \frac{W}{T_i} \left(\frac{L \cdot SA_{NS}}{B} - \frac{1}{2} \right), \frac{SA_{NS} \cdot W}{4V_i} \right\} \quad (7)$$

The height of COM (L) can be substituted with the total height (H) of the object, depending on the shape. For objects that have similar shape to Figures 14a and 14b, $L = H/2$ and $L = 2H/3$, respectively.

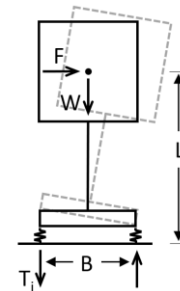


Figure 15: Illustration of the forces experienced by the artefact in an earthquake.

DETERMINATION OF THE DESIGN SEISMIC COEFFICIENT

The last parameter that needs to be determined in order to confirm the number of adhesive dots is the design seismic coefficient for the non-structural component (SA_{NS}). This section describes the procedure to obtain SA_{NS} for both fixed substrate and isolated substrate scenarios. In the example demonstrated below, a specific modal superposition method is adopted to determine the floor response spectra. However, if one wish to use a different method to compute floor response spectra, guidance is also given for which periods and scaling factor to select.

Seismic Demand for Adhesives on Fixed Substrates

Ground elastic response spectra from NZS 1170.5:2004 are used as the basis to design earthquake actions for buildings [21]. For non-structural components (artefacts) that are located at higher levels, the effects of filtering and higher mode amplification should be accounted for. To this extent, floor response spectra are developed for non-structural components based on the building response and should therefore be dependent on the ground elastic response spectra. Different countries have different means of computing ground elastic response spectra and floor response spectra. In New Zealand, the NZS1170.5:2004 [21] standard recommends using the by-parts approach in which simplified equations are provided for estimating demands at different levels. A number of researchers have highlighted shortcomings with the current code approaches [22–24].

To overcome these limitations, a practice-oriented modal superposition method has been recently proposed by Haymes et al. [25] and is adopted here to determine the design seismic coefficient for museum artefacts. As described by Equation 8, the elastic floor acceleration response spectrum at a certain floor, j , is the maximum value of the square root of sum of squares (SRSS) combination of the modal acceleration spectrum and ground acceleration spectrum, an example is demonstrated later in Figure 17.

$$SA_{NS} = \max\left[\sqrt{\sum_i SA_{floor,i,j}(T_{NS}, \xi_{NS})^2}, SA_{ground}(T_{NS}, \xi_{NS})\right] \quad (8)$$

where, SA_{NS} is the design seismic coefficient for the non-structural component, i is the i -th mode of vibration of the structure, and j is the floor of interest (i.e. the floor where non-structural component is located). For higher modes effects, the first three modes of vibration are considered sufficient. While this estimate could be inaccurate, the approach of Haymes et al. [25] does make some allowance for uncertainty in the building characteristics. $SA_{ground}(T, \xi)$ is the ground acceleration response spectrum that is dependent on the site location. In New Zealand, information of SA_{ground} can be found in NZS1170.5:2004. $SA_{floor}(T, \xi)$ is the floor acceleration response spectrum that is affected by the structural properties. In order to compute SA_{NS} , one firstly needs to determine the period (T_{str}) and the equivalent viscous damping (ξ_{str}) of the structure. T_{NS} is the period of the non-structural component, whereas ξ_{NS} is the equivalent viscous damping of the non-structural component.

In the application of this approach to museum artefacts, additional simplifications are made to reduce the technical complexity and allow people who are not from an engineering background to apply such a method. Without knowing the construction details of a structure, the fundamental period of a building is assumed to be $T_{str} = 0.1 \times \text{total number of storeys}$. A 5% equivalent viscous damping ($\xi_{str} = 5\%$) is assumed for conventional structures. Although the equivalent viscous damping can vary depending on the building characteristics and level of shaking, it was argued to have a relatively small effect on non-structural components, therefore, 5% is assumed for simplicity [26]. The process of determining T_{NS} is iterative. It depends on the number of applied adhesive dots and can be computed based on the shear stiffness reported in Table 2. T_{NS} is generally assumed to be less than 0.1s. Due to the large variation observed in shear stiffness results, it is recommended to consider a range of periods (i.e. $T_{NS} = 0 - 0.1$ s) and select the largest design seismic coefficient. The equivalent viscous damping for the non-structural component is typically found to be around 2 to 5% [26]. For simplicity, in this work it is assumed that 5% equivalent viscous damping is sufficiently accurate for the artefacts.

An application of this method is demonstrated through an example. A vase is displayed on the top floor of a four-storey building in Christchurch and is anchored using adhesive dots only. The floor response spectra for a seismic intensity with a 1

in 500 return period are plotted in Figure 17. Note that in New Zealand, buildings are designed using a limit state design approach, where the Ultimate Limit State (ULS) aims to ensure the probability of collapse of a building is acceptable (NZS1170.5:2004, 2004). A common return period for ULS is 500 years. Figure 17a presents the floor acceleration spectrum obtained using the method proposed by Haymes et al. [25]. The floor acceleration SA_{NS} is essentially the envelope of the ground response, and first, second, and third mode responses. Between periods 0 to 0.1 s, the maximum acceleration the vase will experience is 2.3 g (i.e., $SA_{NS} = 2.3$). The displacement of the vase in this case is negligible since its period is short. However, the floor displacement response spectrum is still plotted in Figure 17b and will be considered later for a seismically isolated vase.

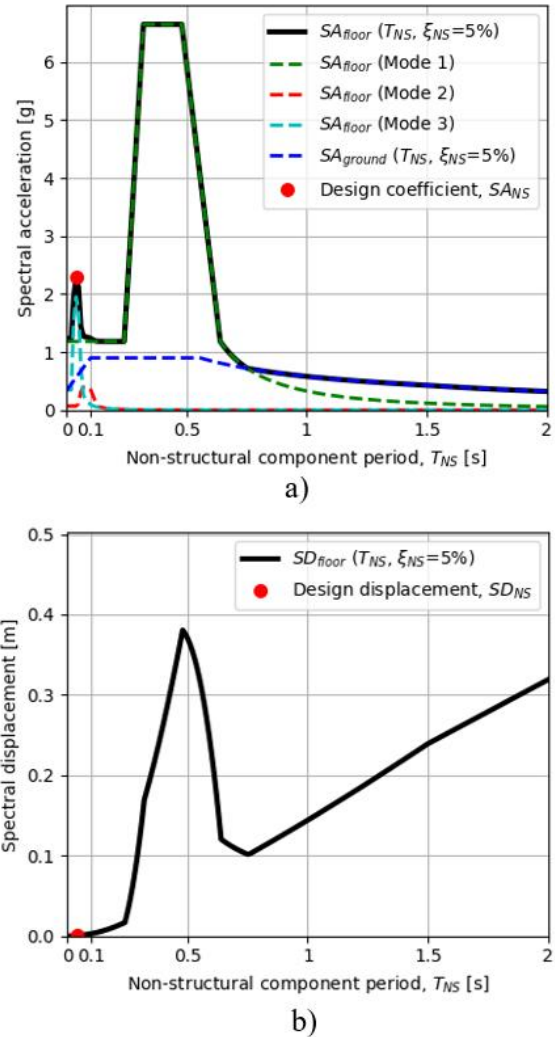


Figure 16: Floor response spectra and design demands for artefacts on fixed substrates, at the top floor of a four-storey building in Christchurch: a) spectral acceleration, b) spectral displacement.

Seismic Demand for Adhesives on Isolated Substrates

As Equation 7 suggests, a heavier object will have a higher seismic force demand, and the required number of adhesive dots can become impractical to provide. A solution to this is using isolated substrate which reduces the base shear force and elongates the system's period. In the design of seismically isolated buildings, it is required to check the building performance using both lower and upper bound friction coefficients [27–29]. Because the lower bound generally governs the displacement demand and the upper bound tends to dominate force demand. The same logic can be applied to the

design of seismically isolated museum artefacts. Based on the friction test results from Figures 12 and 14, a lower bound friction coefficient of 0.06 and an upper bound of 0.25 are suggested. Note these lower and upper bound friction coefficients are suitable for PTFE-stainless steel and PTFE-glass.

Recognising that for an artefact anchored on an isolated substrate, the base shear is limited by the friction force of the isolated substrate. Equalling the base shear and the friction force and then normalising by its weight, one will find that the seismic design coefficient (SA_{NS}) is equal to the friction coefficient (μ). However, base isolation also means that the isolated substrate will slide during an earthquake. Floor response spectra are useful to determine how much it slides and the approach from Haymes et al. [25] is also considered applicable in this case but with a few modifications. Firstly, adding an isolation device changes the non-structural component's equivalent viscous damping. In the case of a flat sliding bearing, Priestley et al. [30] proposed an equation for equivalent viscous damping.

$$\xi_{eq} = 0.05 + 0.670 \left(\frac{\mu - 1}{\mu \pi} \right) \quad (9)$$

Equation 9 is a function of ductility, and the ductility of a flat sliding bearing is large enough that Equation 9 yields an equivalent viscous damping of 26% when sliding occurs. Non-linear time history analyses can be performed to obtain more accurate results [31]. However, considering that the proposed seismic protection method has some simplifications and assumptions, Equation 9 is considered to provide adequate results and ensures an adequate level of simplification. Equation 9 should be used together with the damping reduction factor (Equation 10) provided in the draft version of Eurocode 8 [28] for reasoning explained in [30,32,33].

$$\eta = \sqrt{\frac{7}{2 + \xi_{eq}}} \quad (10)$$

Knowing that ξ_{eq} is 26% for a flat sliding bearing, the damping reduction factor, η is calculated to be 0.5 according to Equation 10. Now consider the example of the vase located on the top floor of a four-storey building in Christchurch, but this time the vase is anchored on the isolated substrate. The floor response spectra should be similar to Figure 17 but with a scaling factor of $\eta = 0.5$ to account for the 26% damping, shown in Figure 18.

As mentioned previously, the friction coefficient, μ (hence the seismic design coefficient, SA_{NS}) varies from 0.06 to 0.25, which correspond to effective periods, T_{eff} of 4.0 s and 1.2 s, respectively, on the damped floor acceleration spectrum, shown in Figure 18a. Similarly, these effective periods are labelled on the damped floor displacement spectrum as shown in Figure 18b. A range of displacement demands, SD_{NS} can be estimated, which are between 90 mm to 240 mm. In conclusion, to incorporate the uncertainties associated with isolated substrate properties, both upper and lower bound friction coefficients are checked. The upper bound governs the seismic design coefficient, which is $SA_{NS} = 0.25$, this value should be used to determine the number and size of adhesives required for anchorage. The low bound governs the displacement demand, which is $SD_{NS} = 240$ mm, and this value should be considered as the clearance around the isolated substrate to avoid impact with the surroundings.

Seismic Demand for Generic Floor Response Spectra

The example demonstrated above adopted a modal superposition method [25] to determine the floor response spectra. The proposed seismic protection approach can also be

applied to other generic floor response spectra, summarised as follows.

In the case of anchoring the artefact to a fixed substrate, using the 5% damped (scaling factor = 1) floor response spectra. The design seismic coefficient is the largest value within a non-structural component period range of 0 to 0.1s.

In the case of anchoring the artefact to an isolated substrate, using the 26% damped (scaling factor = 0.5) floor response spectra. Determine the effective periods corresponding to the lower and upper bound coefficient of friction from the scaled floor acceleration spectrum. The design seismic coefficient is the larger of $SA_{NS}(T_{eff1})$ and $SA_{NS}(T_{eff2})$, which is also the upper bound friction coefficient. The required clearance is the larger of $SD_{NS}(T_{eff1})$ and $SD_{NS}(T_{eff2})$.

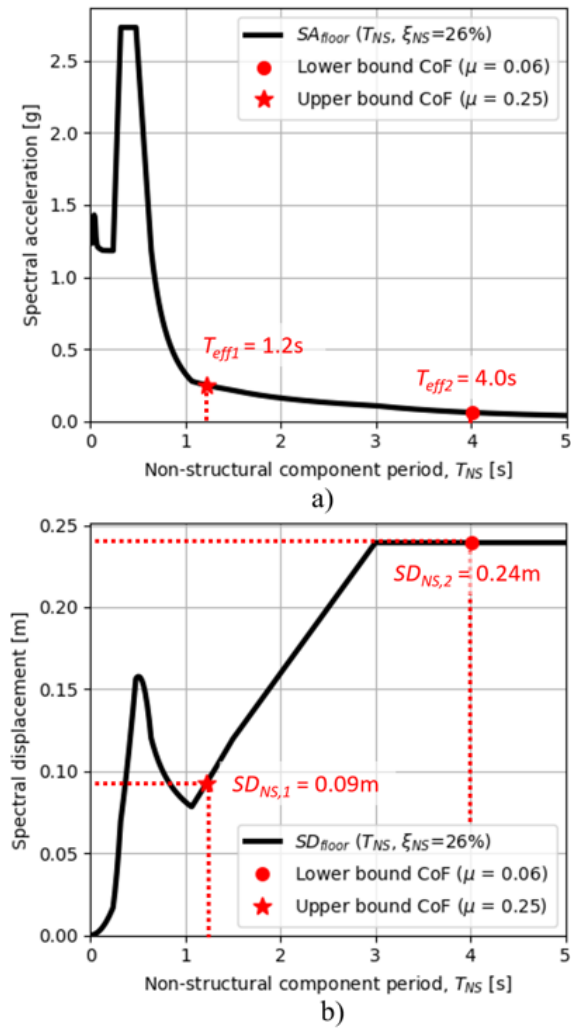


Figure 17: Damped floor response spectra at the top floor of a four-storey building in Christchurch: a) spectral acceleration, b) spectral displacement.

VALIDATION OF THE PROPOSED SEISMIC PROTECTION METHODS

To validate the proposed design methods, a shake table test was set up to simulate a recorded acceleration time series. This time series represented the floor response and had a peak acceleration of 0.6 g. The floor response spectra were computed in order to estimate the seismic design coefficient, SA_{NS} and the displacement demand, SD_{NS} . The test setup is shown in Figure 19, where four terracotta pots were anchored onto painted MDF substrates. T-1, T-2, and T-3 were tested under fixed-base conditions. T-4 was base-isolated and allowed to

slide freely on a glass bearing. Each terracotta pot had a height of 205 mm, a base width of 95 mm, and weight of 11.5 N. The narrow rim at the base allowed a maximum of 3 mm diameter adhesive dots. From Equation 7, three Lascaux 303HV D3 were required in each quadrant to anchor the terracotta pot on the fixed substrate (T-3), and one Lascaux 303HV D3 was required to anchor it on the isolated substrate (T-4). As a comparison, two more terracotta pots (T-1 and T-2) were tested with less adhesives, see Figure 19. Test outcomes showed that T-3 and T-4 survived the simulated earthquake shaking as expected. T-2 with one less adhesive dot in each quadrant also survived which suggested the proposed method still has some conservatism. T-1 fell down and was damaged, demonstrating that seismic protection was needed.

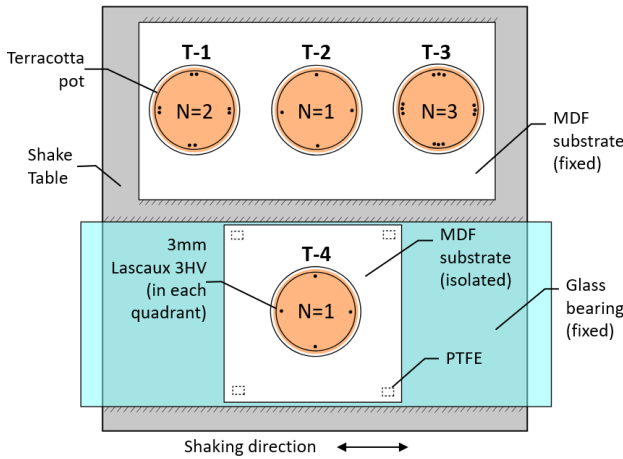


Figure 18: Shake table test setup adopted to validate proposed seismic protection solutions.

SUMMARY OF THE PROPOSED SEISMIC PROTECTION METHODS

Two seismic protection methods are investigated: 1) applying adhesives to small artefacts; and 2) inserting an isolation substrate to medium sized artefacts in addition to adhesives. Figure 20 presents the overview of the proposed framework including the assumptions made to simplify the process, calculations of required number of adhesive dots, as well as the clearance required for the isolation platforms in the event that these are deemed necessary.

Most museums and galleries in New Zealand are around two storeys in height. Taller buildings like the Museum of New Zealand Te Papa Tongarewa in Wellington and Christchurch Art Gallery Te Puna o Waiwhetū generally have low damage seismic technologies applied to reduce the seismic demand. Following the proposed methods in this study, in particular Equation 7, one can plot charts similar to Figures 21–25 which summarise the requirements of applying adhesive dots at a given location in the building. In these plots, L/B is the ratio between the object’s COM height and base width, and N is the number of dots required in each quadrant (hence the total number of dots is $4N$). Beyond a certain number of dots alternative solutions such as the base-isolated platform is recommended. Guidance of applying Lascaux 303HV adhesive dots in six major cities in New Zealand including Christchurch, Auckland, Dunedin, Tauranga, Hamilton, and Wellington are presented in Figures 21–25. These plots are derived for an artefact that is located on the second floor in a two-storey building. But they are also applicable for any artefact that is located on the first (ground) floor in a two-storey building or in a one-storey building.

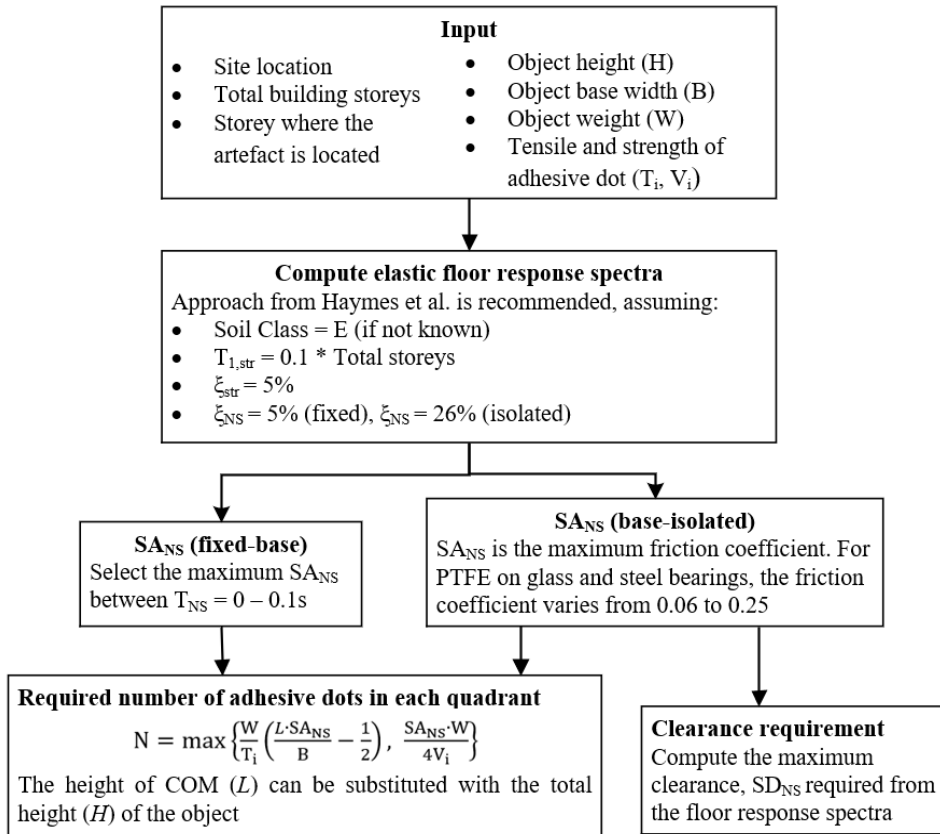


Figure 19: A flowchart describing the process to identify the required number of adhesive dots and characteristics of base-isolated platform.

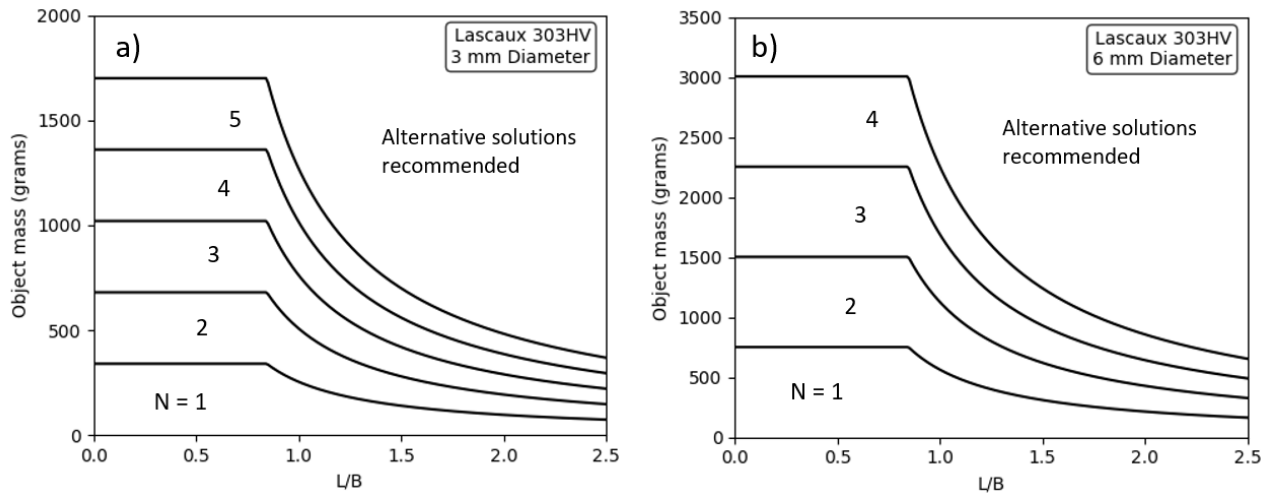


Figure 20: Guidance for applying adhesive dots to an object at the top storey in a two-storey building in Christchurch: a) Lascaux 303 HV 3 mm diameter, and b) Lascaux 303 HV 6 mm diameter.

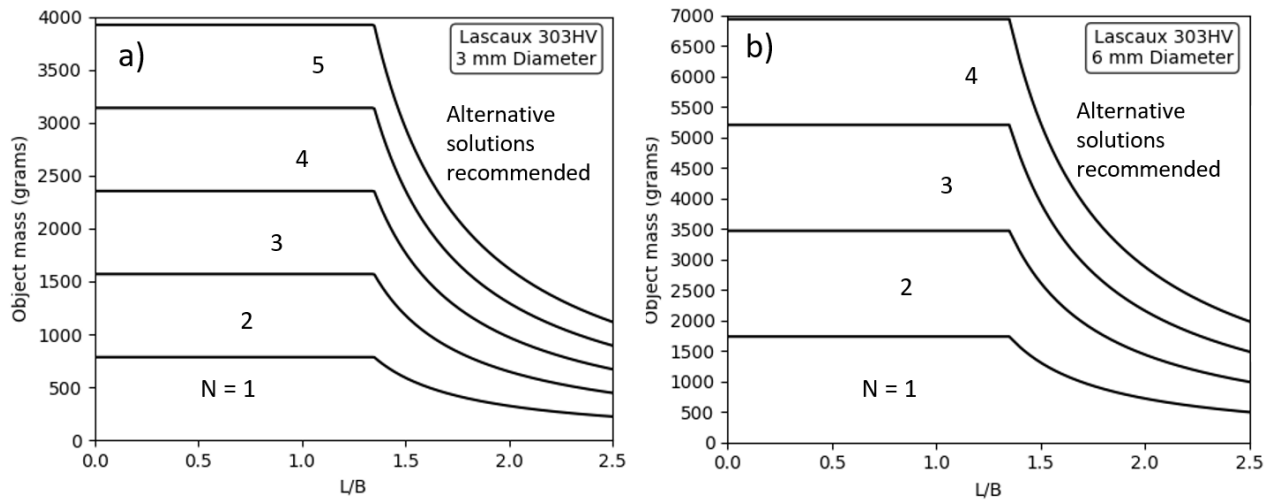


Figure 21: Guidance for applying adhesive dots to an object at the top storey in a two-storey building in Auckland and Dunedin: a) Lascaux 303 HV 3 mm diameter, and b) Lascaux 303 HV 6 mm diameter.

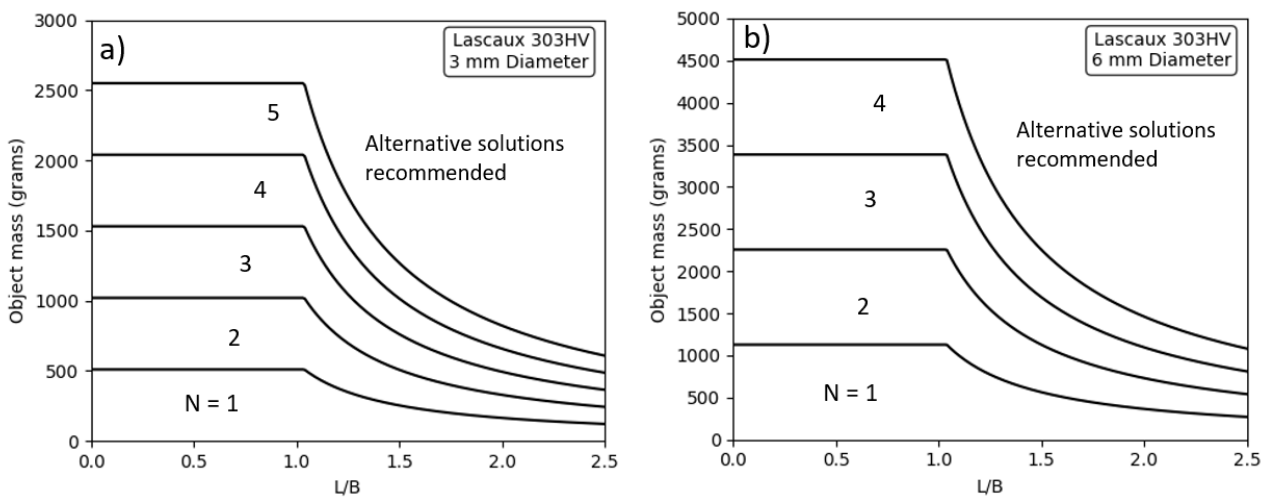


Figure 22: Guidance for applying adhesive dots to an object at the top storey in a two-storey building in Tauranga: a) Lascaux 303 HV 3 mm diameter, and b) Lascaux 303 HV 6 mm diameter.

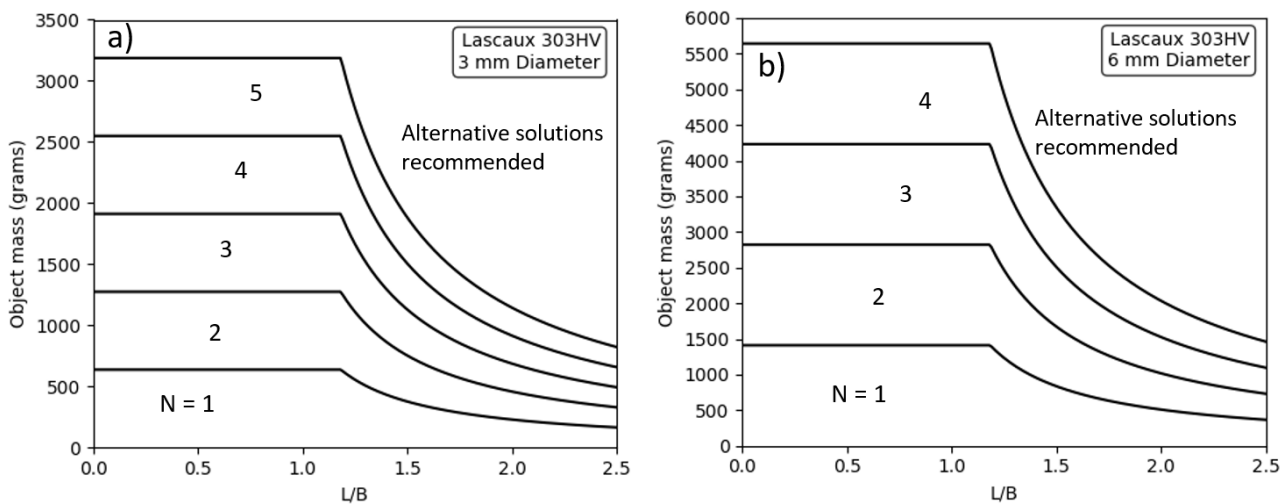


Figure 23: Guidance for applying adhesive dots to an object at the top storey in a two-storey building in Hamilton: a) Lascaux 303 HV 3 mm diameter, and b) Lascaux 303 HV 6 mm diameter.

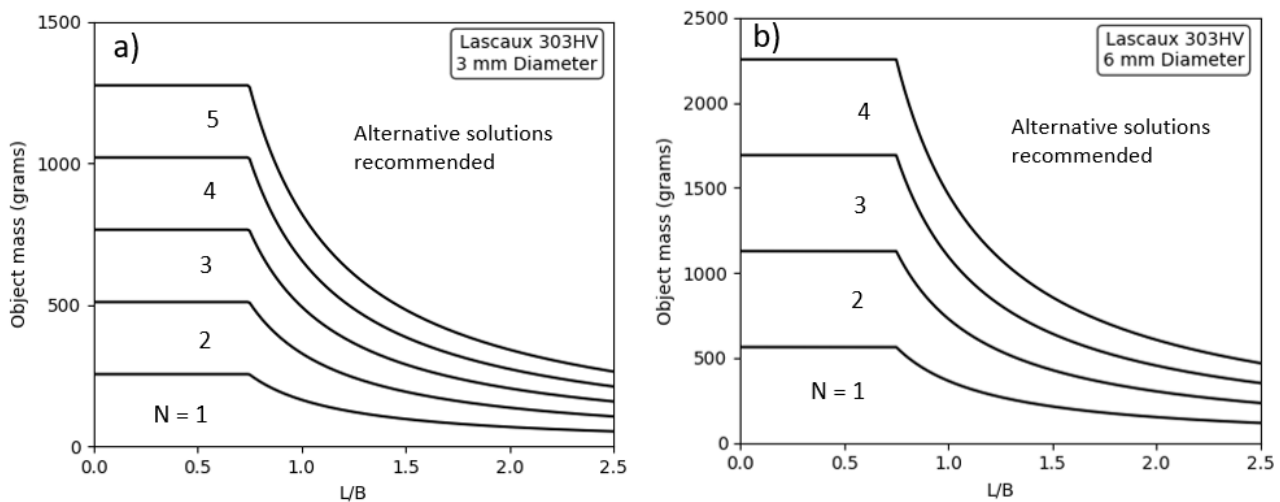


Figure 24: Guidance for applying adhesive dots to an object at the top storey in a two-storey building in Wellington: a) Lascaux 303 HV 3 mm diameter, and b) Lascaux 303 HV 6 mm diameter.

CONCLUSION

The overall goal of this research is to investigate seismic protection methods to the museum artefacts. Both experiential tests and theoretical derivation are used to support the proposed methods. The following conclusions are drawn:

- Using pre-made adhesive dots to anchor small artefacts. Guidance is provided to determine the size and number of adhesives required for an artefact to survive design-level earthquake shaking.
- For medium objects, a simple affordable base-isolated substrate is proposed in addition to adhesive dots. The base-isolated substrate is comprised of a rigid substrate that supports the objects and four PTFE flat sliders glued at the base. A clearance around the base-isolated substrate is recommended to avoid impact with the surroundings. Although this base-isolated substrate is proposed for relatively larger artefacts, it is also feasible to isolate a group of small artefacts on a single platform, given that the small artefacts are properly anchored to avoid falling into each other during the sliding movement.
- Direct tension and shear tests were conducted to determine the tensile and shear strength of the pre-prepared adhesives. As a result, Lascaux 303HV is recommended due to its availability, strength, and the small residual it leaves on artefacts. To apply Lascaux 303HV adhesives it is recommended that the object and substrate surfaces be

cleaned and dried. Adhesive dots should be applied as closely as possible to avoid distributing load unevenly.

- Unidirectional and cyclic loading tests were conducted to determine the coefficient of friction of the base-isolated substrate for artefacts. The observation suggests that PTFE sliding on glass has an overall better performance, due to its low coefficient of friction (0.06–0.25), durability, aesthetics, and cost.
- The proposed methods have been validated with a shake table test where a set of vases with different protection measures were subjected to a real earthquake record. The results obtained confirmed that the proposed solutions work adequately and provide a reasonably conservative level of protection.
- This base-isolated substrate is proposed as an alternative. It is also feasible to isolate a group of small artefacts on such a base-isolated substrate given that the small artefacts are properly anchored to avoid knocking into each other during sliding movement.

The research investigated some of the factors that can affect the tensile and shear strength of the adhesives such as the quantity and strain. However, there are other factors that were not investigated in this study, for example, how would the adhesive strength change with time (aging effect)? And how would the strength change if more pressure is applied between artefact and substrate during installation (i.e. similar to applying pressure to

a command hook)? In addition, future research should also consider factors that affect the seismic demand. For instance, how would the seismic demand change if the artefact is displayed on cabinet, and the effects of vertical acceleration. The application of the proposed isolation device for large artefacts such as statues will need to be further investigated and validated.

ACKNOWLEDGMENTS

The authors would like to thank the University of Canterbury for the financial support and providing lab equipment. The authors also appreciate Canterbury Museum for providing test specimens and knowledge on museum conservation.

This project was partially supported by QuakeCoRE, a New Zealand Tertiary Education Commission-funded Centre. This is QuakeCoRE publication number 0802. This project is also partly supported by the Resilience to Nature's Challenges Built Environment theme.

REFERENCES

- Parisi F and Augenti N (2013). "Earthquake damages to cultural heritage constructions and simplified assessment of artworks". *Engineering Failure Analysis*, **34**, 735–760. <https://doi.org/10.1016/j.engfailanal.2013.01.005>
- Hare J, Oliver S and Galloway B (2012). "Performance objectives for low damage seismic design of buildings". *Annual Conference of the New Zealand Society for Earthquake Engineering*, Paper 035, Christchurch, New Zealand. <https://www.nzsee.org.nz/db/2012/Paper035.pdf>
- Campbell P (2018). "Proposed low damage design guidance - A NZ approach". *17th U.S.-Japan-New Zealand Workshop on the Improvement of Structural Engineering and Resilience*, Queenstown, New Zealand. <https://www.atcouncil.org/docman/atc-15-16-papers/154-p1-02-campbell/file>
- Rashid M, Dhakal RP and Sullivan TJ (2021). "Seismic design of acceleration-sensitive non-structural elements in New Zealand: State-of-practice and recommended changes". *Bulletin of the New Zealand Society for Earthquake Engineering*, **54**(4): 243-262. <https://doi.org/10.5459/bnzsee.54.4.243-262>
- Ning X, Dai J, Bai W, Yang Y and Zhang L (2018). "Seismic protection of cabinet stored cultural relics with silicone dampers". *Shock and Vibration*. **2018**: 3501848. <https://doi.org/10.1155/2018/3501848>
- Morton J (2006). "A preliminary comparison of the strength of two waxes for securing objects against earthquake damage (No. 17)". Te Papa Museum of New Zealand. https://www.tepapa.govt.nz/sites/default/files/tuhinga.17.2.006.pt5_p61-68.morton.pdf
- Fragiadakis M, DiSarno L, Saetta A and Berto L (2020). "Experimental seismic assessment and protection of museum artefacts". *XI International Conference on Structural Dynamics*, 3381–3396, 23-26 November, Athens, Greece. <https://doi.org/10.47964/1120.9277.20698>
- Sorace S and Terenzi G (2015). "Seismic performance assessment and base-isolated floor protection of statues exhibited in museum halls". *Bulletin of Earthquake Engineering*, **13**(6): 1873–1892. <https://doi.org/10.1007/s10518-014-9680-3>
- Pellecchia D, Sessa S, Vaiana N and Rosati L (2020). "Comparative assessment on the rocking response of seismically base-isolated rigid blocks". *Procedia Structural Integrity*, **29**: 95-102. <https://doi.org/10.1016/j.prostr.2020.11.144>
- Pellecchia D, Feudo SL, Vaiana N, Dion JL and Rosati L (2022). "A procedure to model and design elastomeric-based isolation systems for the seismic protection of rocking art objects". *Computer Aided Civil and Infrastructure Engineering*, **37**: 1298–1315. <https://doi.org/10.1111/mice.12775>
- Velagapudi N, Fryer E, Murray S, Ramsdale K, Denize S and Adshead S (2021). "Finding a temporary adhesive for securing objects for display in earthquake-prone regions". *Studies in Conservation*, 1–7. <https://doi.org/10.1080/00393630.2021.1984091>
- Dayyoub T, Maksimkin AV, Kaloshkin S, Kolesnikov E, Chukov D, Dyachkova TP and Gutnik I (2018). "The structure and mechanical properties of the UHMWPE films modified by the mixture of Graphene Nanoplates with Polyaniline". *Polymers*, **11**(1). <https://doi.org/10.3390/polym11010023>
- Campbell TI, Kong WL and Manning DG (1990). "Laboratory investigation of the coefficient of friction in the Tetrafluorethylene slide surface of a bridge bearing". *Transportation Research Record 1275*: 45-52. <https://onlinepubs.trb.org/Onlinepubs/trr/1990/1275/1275-007.pdf>
- Dong C (2022). "Adhesive Test", in *Seismic protection of artefacts with adhesives and base-isolation*. DesignSafe-CI. <https://doi.org/10.17603/ds2-jtb9-9w60>
- Porter K, Kennedy R and Bachman R (2007). "Creating fragility functions for performance-based earthquake engineering". *Earthquake Spectra*, **23**(2): 471–489. <https://doi.org/10.1193/1.2720892>
- Lilliefors HW (1967). "On the Kolmogorov-Smirnov test for normality with mean and variance unknown". *Journal of the American Statistical Association*, **62**(318): 399–402. <https://doi.org/10.1080/01621459.1967.10482916>
- Dong C (2022). "Unidirectional Load Friction Test of PTFE", in *Seismic protection of artefacts with adhesives and base-isolation*. DesignSafe-CI. <https://doi.org/10.17603/ds2-smfe-wy17>
- Stanton J and Taylor J (2010). "Friction coefficients for stainless steel (PTFE) teflon bearings". Wisconsin Highway Research Program. <https://doi.org/10.2307/2283970>
- Calabrese A, Quaglini V, Strano S and Terzo M (2020). "Online estimation of the friction coefficient in sliding isolators". *Structural Control and Health Monitoring*, **27**(3). <https://doi.org/10.1002/stc.2459>
- Dong C (2022). "Cyclic Load Friction Test of PTFE", in *Seismic protection of artefacts with adhesives and base-isolation*. DesignSafe-CI. <https://doi.org/10.17603/ds2-4ww3-5f22>
- Standards New Zealand (2004). "NZS 1170.5 Structural Design Actions - Part 5: Earthquake Actions - New Zealand". Standards New Zealand, Wellington, New Zealand. <https://www.standards.govt.nz/shop/nzs-1170-52004/>
- Sullivan TJ, Martino CP and Nascimbene R (2013). "Towards improved floor spectra estimates for seismic design". *Earthquakes and Structures*, **4**(1): 109–132. <https://doi.org/10.12989/eas.2013.4.1.109>
- Lim E and Chow N (2015). "Review of approaches for analysing secondary structures in earthquakes and evaluation of floor response spectrum approach". *International Journal of Protective Structures*, **6**(2): 237–261. <https://doi.org/10.1260%2F2041-4196.6.2.237>

- 24 Uma SR, Zhao JX and King AB (2009). "Floor response spectra for ultimate and serviceability limit states of earthquakes". *Structures Congress*, Apr 30-2 May, Austin, Texas, US. [https://doi.org/10.1061/41031\(341\)64](https://doi.org/10.1061/41031(341)64)
- 25 Haymes K, Sullivan T and Chandramohan R (2020). "A practice-oriented method for estimating elastic floor response spectra". *Bulletin of the New Zealand Society for Earthquake Engineering*, **53**(3): 116–136. <https://doi.org/10.5459/bnzsee.53.3.116-136>
- 26 Applied Technology Council (2018). "*Recommendations for Improved Seismic Performance of Nonstructural Components*". Technical Report, Applied Technology Council, Redwood City, CA. <https://doi.org/10.6028/NIST.GCR.18-917-43>
- 27 ASCE/SEI (2017). "*Minimum Design Loads and Associated Criteria for Buildings and Other Structures: ASCE/SEI 7-22*". American Society of Civil Engineers. <https://doi.org/10.1061/9780784415788>
- 28 British Standards Institution (1996). "*Eurocode 8: Design of Structures for Earthquake Resistance – Part 1: General Rules, Seismic Actions and Rules for Buildings*". London: British Standards Institution.
- 29 NZSEE/MBIE (2019). "*Guideline for the Design of Seismic Isolation Systems for Buildings*". New Zealand Society of Earthquake Engineering. <https://www.nzsee.org.nz/wp-content/uploads/2019/06/2825-Seismic-Isolation-Guidelines-Digital.pdf>
- 30 Priestley MJN, Calvi GM and Kowalsky MJ (2007). *Displacement-based Seismic Design of Structures*. IUSS Press. [https://doi.org/10.1016/S0141-0296\(98\)00093-5](https://doi.org/10.1016/S0141-0296(98)00093-5)
- 31 Vaiana N, Sessa S, Paradiso M and Rosati L (2019). "Accurate and efficient modeling of the hysteretic behavior of sliding bearings". *Proceedings of the 7th International Conference on Computational Methods in Structural Dynamics and Earthquake Engineering (COMPdyn)*, Crete, Greece. <https://doi.org/10.7712/120119.7304.19506>
- 32 Pennucci D, Sullivan TJ and Calvi GM (2011). "Displacement reduction factors for the design of medium and long period structures". *Journal of Earthquake Engineering*, **15**(sup1): 1–29. <https://doi.org/10.1080/13632469.2011.562073>
- 33 Sullivan TJ, Priestley MJN and Calvi GM (2012). *A Model Code for the Displacement-based Seismic Design of Structures: DBD12*. IUSS Press.